

---

EFDA–JET–CP(04)03-17

X. Garbet, P. Mantica, C. Angioni, E. Asp, Y. Baranov, C. Bourdelle,  
R. Budny, F. Crisanti, G. Cordey, L. Garzotti, N. Kirneva, D. Hogewej,  
T. Hoang, F. Imbeaux, E. Joffrin, X. Litaudon, A. Manini, D.C. McDonald,  
H. Nordman, V.Parail, A. Peeters, F. Ryter, C. Sozzi, M. Valovic, T. Tala,  
A. Thyagaraja, I. Voitsekhovitch, J. Weiland, H. Weisen, A. Zabolotsky  
and JET EFDA Contributors

# Physics of Transport in Tokamaks

---



# Physics of Transport in Tokamaks

X. Garbet<sup>1</sup>, P. Mantica<sup>2</sup>, C. Angioni<sup>3</sup>, E. Asp<sup>1</sup>, Y. Baranov<sup>4</sup>, C. Bourdelle<sup>1</sup>,  
R. Budny<sup>5</sup>, F. Crisanti<sup>6</sup>, G. Cordey<sup>4</sup>, L. Garzotti<sup>7</sup>, N. Kirneva<sup>8</sup>, D. Hogeweij<sup>9</sup>,  
T. Hoang<sup>1</sup>, F. Imbeaux<sup>1</sup>, E. Joffrin<sup>1</sup>, X. Litaudon<sup>1</sup>, A. Manini<sup>3</sup>, D.C. McDonald<sup>4</sup>,  
H. Nordman<sup>10</sup>, V. Parail<sup>4</sup>, A. Peeters<sup>3</sup>, F. Ryter<sup>3</sup>, C. Sozzi<sup>2</sup>, M. Valovic<sup>4</sup>, T. Tala<sup>11</sup>,  
A. Thyagaraja<sup>4</sup>, I. Voitsekhovitch<sup>4</sup>, J. Weiland<sup>10</sup>, H. Weisen<sup>12</sup>, A. Zabolotsky<sup>12</sup>  
and JET EFDA Contributors\*

<sup>1</sup>Assoc. Euratom-CEA sur la Fusion, CEA Cadarache, 13108 St Paul-Lez-Durance, France.

<sup>2</sup>Istituto di Fisica del Plasma EURATOM-ENEA/CNR, via Cozzi 53, 20125 Milano, Italy.

<sup>3</sup>MPI für Plasmaphysik, EURATOM-Assoz., D-8046 Garching bei München, Germany

<sup>4</sup>EURATOM/UKAEA, Culham Science Centre, Abingdon OX14 3DB, United Kingdom.

<sup>5</sup>PPPL, Princeton University, P.O. Box 451, Princeton, NJ 08543, USA.

<sup>6</sup>Assoc. EURATOM-ENEA sulla Fusione, Via Enrico Fermi 27, 00044 Frascati, Italy.

<sup>7</sup>EURATOM-ENEA-CNR Association, Istituto Gas Ionizzati, Padova, Italy

<sup>8</sup>RRC Kurchatov Institute, Moscow, Russia

<sup>9</sup>FOM-Instituut voor Plasmafysica, Associatie Euratom-FOM, Nieuwegein, The Netherlands

<sup>10</sup>Chalmers Univ. of Technology and EURATOM-VR Assoc, S-41296 Göteborg, Sweden.

<sup>11</sup>Association EURATOM-TEKES, VTT Processes, FIN-02044 VTT, Finland.

<sup>12</sup>Assoc. Euratom-Confédération Suisse, CRPP, EPFL, CH-1015 Lausanne, Switzerland

\* See annex of J. Pamela et al, "Overview of Recent JET Results and Future Perspectives", Fusion Energy 2002 (Proc. 19<sup>th</sup> IAEA Fusion Energy Conference, Lyon (2002).

“This document is intended for publication in the open literature. It is made available on the understanding that it may not be further circulated and extracts or references may not be published prior to publication of the original when applicable, or without the consent of the Publications Officer, EFDA, Culham Science Centre, Abingdon, Oxon, OX14 3DB, UK.”

“Enquiries about Copyright and reproduction should be addressed to the Publications Officer, EFDA, Culham Science Centre, Abingdon, Oxon, OX14 3DB, UK.”

## **ABSTRACT**

This paper is an overview of recent results relating to turbulent particle and heat transport, and to the triggering of Internal Transport Barriers. The dependence of the turbulent particle pinch velocity on plasma parameters has been clarified and compared to experiment. Magnetic shear and collisionality are found to play a central role. Analysis of heat transport has made progress along two directions; dimensionless scaling laws, which are found to agree with the prediction for electrostatic turbulence and analysis of modulation experiments, which provide a stringent test of transport models. Finally the formation of Internal Transport Barriers has been addressed by analysing electron transport barriers. It is confirmed that negative magnetic shear, combined with the Shafranov shift, is a robust stabilising mechanism. However, some well established features of internal barriers are not explained by theory.

## **1. INTRODUCTION**

Understanding transport in magnetised plasmas is a subject of utmost importance for the design of future fusion reactors. A vigorous and coordinated effort has been undertaken in Europe to improve our knowledge in this domain. This paper is an overview of recent results that clarify the questions of turbulent particle and heat transport, and conditions for the onset of Internal Transport Barriers. The aim is to compare theoretical and experimental results for each of these topics and to assess the implications for burning plasmas.

Particle transport is a central question, since fusion power increases as the square of the density. Therefore the existence and nature of any process that leads to density peaking deserves attention. Recently theory of turbulent pinches has made significant progress. In particular the role of collisionality and magnetic shear has been clarified. These predictions have been tested against experiments on JET, ASDEX-Upgrade, TORE SUPRA, and TCV.

The understanding of heat transport has advanced along two directions; dimensionless scaling laws and assessment of transport models using heat modulation experiments. Scaling laws are widely used to predict the energy confinement time in next step devices. When written in dimensionless form, they also yield information on the mechanisms that underlie turbulent transport. Profile modelling plays an increasing role for interpreting existing data and for the design of future experiments. Therefore the predictive capability of transport models is a central issue. A powerful mean of testing these models is to use heat modulation experiments. Such experiments have been undertaken, analysed and compared on JET, ASDEX-Upgrade, TORE SUPRA, FTU and TCV.

Finally, triggering Internal Transport Barriers with low power threshold is also a challenge for future devices. This is a delicate question since turbulent transport results from a balance between driving terms (gradients) and a combination of stabilising effects such as magnetic and velocity shears. Electron transport barriers are well suited to study this physics. In this case the electron temperature gradient becomes large, whereas the density, velocity and ion temperature gradients remain small and so, therefore, does the perpendicular velocity shear rate. Magnetic shear is a key

parameter in many cases, as found in JET, ASDEX Upgrade, TORE SUPRA, FTU and TCV. Theory broadly supports this picture. However, some robust features of internal barriers are not understood so far, in particular the role of particular values of the safety factor and the existence of multiple barriers observed at JET. Some possible explanations will be presented in this paper.

The remainder of this paper is organised as follows. Section II briefly presents some general features and properties of drift wave turbulence in core tokamak plasmas. Particle transport is addressed in section III, profile stiffness in section IV and Internal Transport Barriers in section V. A conclusion follows.

## 2. A BRIEF SURVEY OF MICRO-STABILITY AND TURBULENT TRANSPORT.

The guideline of this paper will be a restricted theory of turbulent transport where turbulence is driven by two main micro-instabilities: Ion Temperature Gradient (ITG) driven modes and Trapped Electron Modes (TEM) [1,2] (called here ion and electron modes for simplicity). These modes are unstable in the limit of large wavelengths such that  $k_{\perp}\rho_i < 1$ , where  $k_{\perp}$  is the perpendicular wave number and  $\rho_i$  is the ion Larmor radius. In the non-linear regime, they produce particle, momentum, electron and ion heat transport. The main characteristic of these micro-modes is the existence of an instability threshold. In a Deuterium plasma, and for a given profile of safety factor, the threshold of a pure ion mode (i.e. adiabatic electrons) appears as a critical ion temperature logarithmic gradient  $-R\nabla T_i/T_i$  ( $R$  is the major radius) that depends on the logarithmic density gradient  $-R\nabla n_e/n_e$ , and on the ratio of electron to ion temperature  $T_e/T_i$ . An ion mode usually rotates in the ion diamagnetic direction (the ion diamagnetic velocity is  $\mathbf{V}_{pi}^* = \mathbf{B} \times \nabla p_i / n_i e_i B^2$ , where  $p_i$  is the ion pressure,  $n_i$  the density and  $\mathbf{B}$  the magnetic field). Trapped electron modes usually rotate in the electron diamagnetic direction and are mainly driven through a resonant interaction of the modes with trapped electrons at the precession frequency. The threshold is a critical value of  $-R\nabla T_e/T_e$  that depends on  $-R\nabla n_e/n_e$  and the fraction of trapped electrons  $f_r$ . A separate treatment of ion and electron modes is usually an oversimplification (e.g. in a burning plasma). Still there exist experimental situations where one branch is dominant, for instance when one species is hotter than the others. Figure 1 shows an example of stability diagram in the special case where electron and ion temperatures are equal,  $T_e = T_i$ . Depending on the values of gradient lengths, 0, 1 or 2 modes may be unstable. The sign of the phase velocity is not an unambiguous signature of the type of mode that is excited. Typically, the region of large density gradients in the stability domain is dominated by electron modes, whereas for flat density profile, the first unstable mode is an ion mode. These microinstabilities are, in essence, interchange modes. Well above all thresholds, both branches combine and the growth rate is of the form

$$\gamma_0^2 = f_t \omega_{de}^* \omega_{pe}^* + \omega_{di}^* \omega_{pi}^* \quad (1)$$

where  $\omega_{p\alpha}^* = k_{\theta} V_{pa}^*$  and  $\omega_{d\alpha} = 2k_{\theta} \lambda_{\alpha} V_{da}$  ( $V_{da}$  is the vertical drift velocity  $V_{da} = -2T_d/e_a BR$ ,  $k_{\theta}$  a poloidal wave number). For trapped electrons,  $\lambda_e = 1/4 + 2s/3$  characterises the dependence of the

precession frequency on magnetic shear  $s = d\text{Log}(q)/d\text{Log}(r)$ . For ions,  $\lambda_i = \langle \cos(\theta) + s\theta \sin(\theta) \rangle$ , where the bracket indicates an average over the mode poloidal structure.

First principle transport models such as Weiland [3] or GLF23 [4] models are essentially based on linear stability. They provide quantitative fluxes following two separate steps. The first one is based on a quasi-linear expression of fluxes. Considering for instance the particle flux  $\Gamma_e = \langle n_e v_{Er} \rangle$ , where  $v_E$  is the  $E \times B$  drift velocity (“electrostatic” turbulence), it reads in Fourier space as

$$\Gamma_e = \sum_{k\omega} n_{e, k\omega} \frac{ik_\theta \phi_{k\omega}}{B} \quad (2)$$

where  $\phi_{k\omega}$  and  $n_{k\omega}$  are Fourier components of perturbed electric potential and density. The quasi-linear expression consists in replacing the Fourier component of the density by its linear expression calculated with linearised fluid or kinetic equations. Assuming a convection equation  $\partial_t n_e + \nabla \cdot (n_e v_E) = 0$  and a uniform magnetic field (implying incompressibility  $\nabla \cdot v_E = 0$ ), the recipe given above yields a diffusive law  $\Gamma_e = -D_{ql} dn_e/dr$ . The quasi-linear diffusion coefficient  $D_{ql}$  is given by the expression

$$D_{ql} = \sum_{k\omega} \left| \frac{k_\theta \phi_{k\omega}}{B} \right|^2 \tau_{c, k} \quad (3)$$

where  $\tau_{c, k}$  a correlation time. This expression can be understood as a random walk estimate. A similar exercise can be done for electron (resp. ion) heat flux  $\phi_{Ee} = 3/2 \langle p_e v_{Er} \rangle$  (resp.  $\phi_{Ei} = 3/2 \langle p_i v_{Er} \rangle$ ), leading to a thermal diffusivity  $\chi_{e, i} = 3/2 D_{ql}$ . In fact an advection equation is too simple, and the whole set of fluid or kinetic linearised equations must be kept when calculating the quasi-linear fluxes, as done in the Weiland and GLF23 models. Eq.(3) depends on the level of potential fluctuations, which is unknown at this stage.

The second step consists in using a mixing-length rule to determine the level of fluctuations. The simplest version of this rule is  $e\phi_{k\omega}/T_e = 1/k_\perp L_p$  ( $L_p$  is a pressure gradient length) which can be modified in various ways to account for the complex non linear features of turbulence [2]. Still, this approximation is certainly the weakest part of the derivation of any transport model.

An important feature of turbulent transport is the existence of a similarity principle, which states that 3 dimensionless parameters, among many others, play a central role [5,6]: normalised gyroradius  $\rho^* = \rho_s/a$  ( $a$  is the minor radius,  $\rho_s$  is the gyroradius  $\rho_s = (m_i T_s)^{1/2}/eB$ ), collisionality  $\nu^* = \nu_{ei} qR/\varepsilon_a^{3/2} v_{Te}$  ( $\nu_{ei}$  the electron-ion collision frequency,  $\varepsilon_a = a/R$  the inverse aspect ratio,  $v_{Te}$  is the thermal electron velocity) and plasma beta  $\beta = 2\mu_0 p/B^2$  ( $p$  is total pressure). Turbulence simulations indicate that the scaling law is “gyroBohm” for small enough values of  $\rho^*$ . This means that correlation lengths, correlation times and diffusivity scale respectively as  $\rho_s$ ,  $R/c_s$  and  $r^* T_s/eB$  ( $c_s$  is the acoustic speed  $(T_s/m_i)^{1/2}$ ). The situation is less clear for  $\beta$  and collisionality parameters, because of competing effects. Collisionality has a stabilising effect on electron (TEM) modes because

of electron collisional detrapping. On the other hand, collisional friction damps Zonal Flows [7,8], which are fluctuations of poloidal velocity that reduce turbulent transport. The parameter  $b$  controls both the compression of magnetic surfaces (the Shafranov shift, which is stabilising) and the excitation of electromagnetic instabilities. Hence no  $\beta$  dependence is expected if turbulence is electrostatic and Shafranov shift stabilisation is negligible (typically well below the ideal MHD stability limit).

This overview will address plasmas in L or H-mode. L-mode is the reference case where transport is turbulent everywhere. H-mode is a regime of improved confinement, which results from a quenching of turbulence localised at the plasma periphery. This improvement leads to the formation of a pedestal in density and temperature. Electron and ion modes are expected to control turbulent transport in the core of both L and H-mode plasmas. However the change of boundary conditions affects the domain that is explored in the stability diagram (Fig.1). Since the edge temperature and density become higher at the transition, the logarithmic gradients are lower in the core of H-mode plasmas.

### 3. PARTICLE TRANSPORT

#### 3.1. THEORETICAL UNDERSTANDING OF PARTICLE TRANSPORT

The particle flux of the species ‘ $s$ ’ in a tokamak is traditionally written in the form  $\Gamma_s = -D_s \nabla n_s + V_s n_s$ , where  $V_s$  is the pinch velocity,  $D_s$  the diffusion coefficient and  $n_s$  the density. In plasmas without Neutral Beam Injection (NBI), the ionisation source is mainly peripheral, so that the particle flux in the core vanishes. As a result, the ratio  $V_s/D_s$  is a measure of density peaking  $\nabla n_s/n_s$ . The diffusion coefficient  $D_s$  is found to be larger than the neoclassical (collisional) value in most cases. The situation is less clear for the pinch velocity, since the neoclassical contribution driven by the inductive field, the Ware pinch [9], is rarely negligible in most experiments.

From the theoretical standpoint, two additive terms contribute to the turbulent pinch. One is associated with thermodiffusion [10,11], and predicts a pinch velocity proportional to the temperature logarithmic gradient  $\nabla T_s/T_s$ . The second contribution is proportional to the gradient of magnetic field (or equivalently curvature) and is sometimes called “Turbulence Equi-Partition” term (TEP) [12, 13, 14]. This picture is a somewhat misleading since curvature is not a thermodynamical force, but rather a geometrical effect (in other words the actual thermodynamical forces are the gradients of density and temperature multiplied by a geometry factor). This mechanism received some support from 2D simulations of interchange turbulence [15] and ITG/TEM micro-turbulence [16]. Recently this question was investigated in two papers. One exploits first principles transport models (Weiland and GLF23) [17]. The second one relies on 3D fluid simulations of micro-turbulence [18]. The physical origin of these contributions comes from compressibility that leads to an evolution equation of the density that reads in the collisionless limit as

$$\partial t + v_E \cdot \nabla) n_e = V_{de} \cdot (n_e \nabla \phi - \nabla p_e) \quad (4)$$

The terms on the r.h.s. of this equation lead to non diagonal terms in the quasi-linear flux

$$\Gamma_e = -f_t D_{ql} \left\{ \frac{dn_e}{dr} + C_q \frac{2}{R} n_e - C_T \frac{dT_e}{T_e dr} n_e \right\} \quad (5)$$

The first term is a conventional diffusion, where  $D_{ql}$  is the quasi-linear expression Eq.(3). The second term in expression (5) corresponds to curvature pinch. When ion modes are dominant, trapped electrons behave nearly like test particles. The advection term in the r.h.s. of Eq.(4) must be replaced by the precession frequency of trapped electrons, with the important result  $C_q = \lambda_e = 1/4 + 2s/3$ . Hence the curvature pinch velocity is proportional to the magnetic shear. This is consistent with the Turbulent Equi-Partition (TEP) theory [12,13,14]. When electron modes are dominant,  $C_q = \lambda_i = \langle \cos(\theta) + s\theta \sin(\theta) \rangle$ , i.e. is linked to the ion vertical drift velocity. The dependence on magnetic shear depends on the degree of localisation of modes on the low field side. For ballooned modes, i.e. a turbulence localised close to  $\theta=0$ , a dependence on magnetic shear persists since  $\lambda_i \approx 1 + (s-1/2) \langle \theta^2 \rangle$ .

The third term of Eq.(5) is the contribution of thermo-diffusion. The expression of  $C_T$  is quite intricate. It is positive in a regime dominated by ion modes and decreases when moving to a regime dominated by electron modes. This transition occurs when increasing the ratio of electron to ion heating power. Turbulence simulations indicate that  $C_T$  changes sign when this ratio is high enough as shown in Fig.2.

Collisional detrapping plays an important role in this problem. It was shown in reference [17] that the ratio  $V/D$  decreases with collisionality. This process is effective when the detrapping collision frequency  $\nu_{ei}/\varepsilon$  becomes larger than  $(k_{\perp} \rho_s) c_s / R$ , which measures the electron precession frequency times a typical toroidal wave number. An effective collision frequency was defined in [17] as  $\nu_{eff} = (5/2)^{1/2} n_{ei} R / c_s$ . It is stressed here that the parameter  $\nu_{eff}$  differs significantly from the conventional parameter  $\nu^* = \nu_{ei} q R / \varepsilon_a^{3/2} \nu_{Te}$  for neoclassical transport. A deuterium plasma with  $q = 1.5$ ,  $\varepsilon_a = 0.3$  and  $\nu_{eff} = 1$  is characterised by a parameter  $\nu^*$  of the order of  $0.1$ , i.e. is in the weak collisional regime for neoclassical transport. Also collisionality differs from the ratio between the density and density limit (Greenwald density). A plasma close to the Greenwald density is collisional ( $\nu_{eff} > 1$ ) in present devices, whereas it will be collisionless ( $\nu_{eff} < 1$ ) in ITER.

### 3.2. EXPERIMENTAL RESULTS

Previous experimental results were quite contradictory regarding particle pinch effect. Density profiles were found to be consistent with Ware pinch only in ASDEX-U [19] and JET [20] for plasmas at high density in H-mode. On the other hand, a turbulent pinch was invoked to explain in L-mode density profiles in TCV and TEXTOR [21,22]. Recent experiments have clarified this question in many aspects.

A first class of results deals with plasmas in absence of Ware pinch. Density profiles are peaked in L-mode with zero loop voltage in TORE SUPRA [23], TCV [24] and JET [30]. In TORE SUPRA,

the database includes plasmas with a duration up to 390 seconds, i.e. much larger than a current diffusion time. Thus the inductive field vanishes everywhere, and the Ware pinch velocity as well. The ionisation source was peripheral in those plasmas (no core fuelling). Hence, a turbulent pinch seems to be the most likely explanation for this behaviour (Fig.3). A turbulent pinch was also invoked to explain density profiles in JET [25] and DIII-D [14] L-mode plasmas. At JET, both steady-state regimes and transients (pellet injection) were analysed [25].

Collisionality was found to play a key role in H-mode plasmas. Many plasmas are close to the density limit, in a regime of collisionality where theory predicts small values of  $V/D$  [17]. On the other hand, theory predicts finite density peaking at low collisionality. This appears to be the case in ASDEX-Upgrade [17] and JET [20,26] (Fig. 4). However two difficulties must be mentioned. First the ionisation source is not always negligible in the plasma core (especially at low density). Second any steady-state density profile can be reproduced with a Ware pinch only if the diffusion coefficient is low enough. This lower bound is usually translated into a ratio of diffusion coefficient to electron heat diffusivity  $D/\chi_e$ ,  $\chi_e$  being easier to determine from experiment than  $D$ . In low density JET plasmas the ionisation source alone is not large enough to reproduce the density profile unless  $D/\chi_e$  is smaller than 0.2. This value is lower than predicted by theory [27]. Also analysis of trace Tritium experiments leads to a pinch velocity of Tritium that is close to the neoclassical value at high density and much larger at low density [28,29]. Given uncertainties, these results suggest that density profiles in ITER may be more peaked than assumed. Theory predicts a density gradient length that should be of the order of  $-R\nabla n/n_e = 3$  in the confinement zone [33].

A second class of experiments aims at testing the expression Eq.(5) of particle flux. A series of experiments combining current drive and heating has been undertaken at JET in Lmode to decouple the effects of curvature and thermo-diffusion [26,30]. The result is shown in Fig.5. Density peaking increases with internal inductance, i.e. with the peakedness of current profile. This is consistent with a curvature pinch term that depends on magnetic shear. On the other hand there is no indication of thermodiffusion. The present interpretation is that gradients lie in a region where ion (ITG) and electron (TEM) modes coexist, hence in a region where  $C_T$  is close to zero. This is indeed corroborated by stability analysis. A similar result has been found in TORE SUPRA [31].

A related question is the common observation in tokamaks of density profile flattening with Radio-Frequency heating. Besides MHD effects, which do not seem to play a dominant role, two explanations based on turbulent transport have been proposed up to now:

- an outward pinch due to dominant electron (TEM) turbulence.
- an increase of turbulent diffusion at constant or decreasing pinch velocity [32].

Both explanations are possible, as shown recently in ASDEX-Upgrade [33]. The first one is expected in low collisionality plasmas, with electron heating. Fluid simulations then predict a reversal of the anomalous pinch velocity. The second explanation applies when the pinch velocity is mainly neoclassical since heating should reduce the inductive field and increase the turbulent diffusion. Such behaviour may occur in plasmas at high collisionality, or in the core region, where the anomalous pinch velocity is small [31]. Radio Frequency (RF) heating also flattens impurity profiles (see for instance [34]).

## 4. HEAT TRANSPORT

Predicting the temperature of fusion plasma is obviously crucial for designing a reactor. Two main strategies have been followed up to now. The first line of research relies on the development of scaling laws using a multi-machine database in the frame of the International Tokamak Physics Activity (ITPA). The similarity principle is a powerful tool to reduce the uncertainties on scaling laws [5,6]. The dependence with plasma  $\beta$  and collisionality has been recently revisited, with deep consequences on our theoretical understanding [35,36]. A more sophisticated approach to describe global confinement consists in separating edge and core contribution, leading to two-term scaling laws that have recently been proposed by the ITPA-CDBM group [37]. The second line of action is to use transport models complemented by linear stability analysis and turbulence simulations. Turbulence simulations are time consuming and cannot be used on a routine basis to analyse experiments. However, beyond their usefulness to investigate fundamental questions such as intermittency, turbulence simulations can be used to constrain transport models based on quasi-linear and mixing length rule assumptions (see section II). Examples of transport models are RLW [38], Weiland [2,3], IFS-PPPL [39], GLF23 [4], mixed Bohm-gyroBohm [40], Multi-Mode (MMM) [41], and OHE [42] models. In practice, mixed Bohm-gyroBohm, Weiland and GLF23 models are the most widely used (MMM is a variant of the Weiland model) [43,44,45]. A simpler picture emerges if turbulent transport becomes very large when gradients cross the stability threshold. Profiles then stay marginally stable, i.e. gradients are stuck to their critical value. This is called “profile stiffness” [46]. In practice, only part of the profile is close to marginal stability. This concept is helpful to interpret experiments [47,48,49,50,51,52], when combined with linear stability analysis. The Weiland and GLF23 models provide values of linear growth rates. However they are based on fluid equations, which often predict values for the threshold that are too low. In fact the GLF23 model uses modified fluid equations to correct this drawback. Still the most accurate procedure to calculate growth rates is to solve a kinetic equation to determine the plasma response. The most widely used tools in Europe are the GS2 [53] and Kinezero [54] codes. An intermediate approach between predictive transport modelling and strong profile stiffness consists in using a semi-empirical critical gradient model [55,56,57,58,59]. Such a model is characterised by 3 parameters only and will be used here to illustrate various concepts. The identification of these parameters is made possible by analysing experiments where the heating source is modulated. Profile modulations give access to the heat pulse diffusivity  $\chi_{hp} = \chi + \nabla T \partial \chi / \partial \nabla T$ , and thereby provide a stringent test of transport models [60]. This section presents recent results related to dimensionless scaling laws and analysis of modulation experiments in several devices.

### 4.1. GLOBAL CONFINEMENT - DIMENSIONLESS SCALING LAWS

The IPB(y,2) scaling law for global confinement time in H-mode can be written in the dimensionless form [61]  $B\tau_E \propto \rho^{*-2.7} \beta^{-0.9} \nu^{*-0.01}$  (the magnetic field  $B$  comes from a normalisation of time to cyclotron frequency). A gyroBohm scaling law based on collisionless electrostatic turbulence predicts  $B\tau_E \propto \rho^{*-3}$ . Hence the long established conclusion that scaling law in H-mode is close to the

gyroBohm expectation. On the other hand, the strong dependence on  $\beta$  suggests that electromagnetic effects are important, either in turbulence itself or via MHD effects. This picture has radically changed recently following dedicated experiments in DIII-D and JET [35,36], which lead to the expression  $B\tau_E \propto \rho^*{}^{-3} \beta^{-0.0} \nu^*{}^{-0.35}$ , as illustrated in Fig.6. This new scaling is even closer to the gyroBohm prediction and is consistent with electrostatic turbulent transport. Increasing collisionality is found to be detrimental. This behaviour is somewhat surprising in view of the expected stabilising effect of electron collisional detrapping. Damping of Zonal Flows is a possible explanation. It may also reflect neoclassical effects in the edge pedestal [62].

An alternative approach for H-mode plasmas is a two term scaling law proposed by the ITPA-CDBM group, which separates contributions from the pedestal and bulk plasma [37]. Two versions exist that correspond to different hypotheses on the physics underlying the confinement in the pedestal region. The first one assumes that the edge confinement is controlled by thermal conduction, while the second relies on an MHD  $\beta$  limit within the pedestal region. In terms of accuracy, these two models are equivalent. Considering the model with MHD limited edge, it is found that the scaling law of the energy content in the bulk region is

$$W_{\text{ITPA, bulk, MJ}} = 0.45 M^{0.34} \kappa^{-0.34} \left( \frac{1 + \kappa^2}{2} \right)^{0.68} \epsilon_\alpha^{3.32} R_\theta^{3a-0.6} g_B^{T0.8} n_{a,1}^{90.5} g_{\text{PM}}^{W0.42} \quad (6)$$

where  $\kappa$  is the elongation,  $M$  the mass number,  $n_{a,1}$  the density (in units of  $10^{19} \text{m}^{-3}$ ) and  $P_{MW}$  the additional power (counted in MW). The corresponding normalised confinement time  $B\tau_E$  scales as  $\rho^*{}^{-3} \beta^{0.05}$ . Again it is close to a collisionless electrostatic gyroBohm scaling law.

#### 4.2. PROFILE STIFFNESS AND CRITICAL GRADIENT MODEL

The notion of marginal stability can be illustrated with a simplified transport model. Assuming gyroBohm scaling and electrostatic turbulence (see *section 2*), a critical gradient model is of the form (for each species)

$$\chi_T = \chi_{gB} \left[ \chi_s \left( \frac{-R\partial_r T}{T} - \kappa_c \right) H \left( \frac{-R\partial_r T}{T} - \kappa_c \right) + \chi_0 \right] \quad (7)$$

where  $\chi_{gB} = q^V (T/eB) \rho_s / R$ . Here  $\chi_s$  is a number that characterises the stiffness,  $\kappa_c$ , is the instability threshold, and  $H(x)$  is a Heaviside function. Strong stiffness corresponds to a large value of  $\chi_s$ . It is also assumed that a finite diffusivity persists when the gradient is below the threshold, with an amplitude  $\chi_0$ . The safety factor  $q$  accounts for the improvement of confinement with plasma current. Simulations of ion turbulence [4] and recent dedicated experiments [63] justify this choice. The value  $\nu = 3/2$  is presently the best compromise between various experiments. A detailed analysis of this model shows that the plasma is divided in three regions (see Fig.7): edge, stiff and core regions [39,59]. The temperature is low at the edge and its logarithmic gradient is well above the threshold. In the stiff region the temperature gets higher and its logarithmic gradient is close to the threshold.

An approximate solution is the well-known exponential shape  $T(r) \approx T(r_{gB})e^{\kappa_c(r_{gB}-r)/R}$  where  $r_{gB}$  is the radius of transition between edge and stiff regions. In this region, the temperature increases faster than its gradient (see Fig.8). In the core region the logarithmic derivative of temperature is below the threshold. The transition between stiff and core regions is sharp and is associated with a discontinuity in the heat pulse diffusivity.

Once integrated over the plasma volume a critical gradient model leads to the following expression of core energy content

$$W_{\text{bulk, MJ}} = 0.179 C_{ITPA} \chi_{s, \text{eff}}^{-2/5} \kappa_c^{-4/5} M^{-1/5} \kappa^{7/5} \left(\frac{1+\kappa^2}{2}\right)^{-2/5} \epsilon_\alpha^{8/5} R^3 q_\alpha^{-2/5} B T^{4/5} n_{a, 19}^{3/5} P_{\text{MW}}^{2/5} \quad (8)$$

where  $C_{ITPA}$  depends on edge temperature and the ratio  $\kappa_c \chi_s / \chi_0$ , and the effective stiffness parameter is  $\chi_{s, \text{eff}} = \chi_{s, e} + \chi_{s, i}$ . The factor  $C_{ITPA}$  is not a constant because a two-term scaling law is not consistent with a critical gradient model. In fact separation between edge and core is rigorous if the diffusivity depends on temperature gradient only. However, variations of  $C_{ITPA}$  are moderate [59]. Assuming a threshold  $\kappa_c \approx 5$ , and a reasonable choice of geometry parameters, a comparison of Eqs(6) and (8) leads to  $\chi_{s, \text{eff}}$  in the range 0.3-4.5.

### 4.3. ANALYSIS OF MODULATION EXPERIMENTS

Electron transport has been analysed in detail in ASDEX-Upgrade, JET, FTU, TORE SUPRA and TCV using heat modulation experiments. The analysis has been done using a critical gradient transport model, predictive modelling, and stability analysis. The results obtained with a critical gradient transport model are shown in Fig.8. The thresholds range between 3 and 8, which are typical values expected for micro-modes (Fig.1).

The range of variation of the electron stiffness parameter  $\chi_{s, e}$  is wide ( $\chi_{s, e} \sim 0.15-6$ ). In TCV,  $\chi_{s, e}$  is also in this range (on the lower side). It was noticed in TCV that the critical gradient model does not provide a good fit when the gradient is well above the threshold [58]. Fig.8 indicates that stiffness is sensitive to plasma parameters. At JET, the variation of  $\chi_{s, e}$  appears to be correlated with the logarithmic gradient of ion temperature  $-R \nabla T_i / T_i$  [45] (Fig.9b). This points toward a coupling between electron and ion turbulent transport. An interplay between electron and ion channels can be understood from stability properties of micro-modes. In the hot electron mode, the main instability is an electron mode (TEM), and a critical gradient model of the form Eq.(7) is likely appropriate. When ion heating increases, ion (ITG) modes become unstable and are ultimately the dominant instability. This means that the background diffusivity quantified by  $\chi_0$  in Eq.(7) for electrons represents the contribution of ion modes when they are unstable. However the parametric form that has been chosen for the background diffusivity may not be the right one. Also it is not clear whether contributions of electron and ion modes are additive when both are linearly unstable. Hence Eq.(7) in its present form may not be appropriate in this regime.

Results obtained with predictive modelling and stability analysis can be summarised as follows.

The analysis of modulation experiments in ASDEX-Upgrade using the Weiland model (without off diagonal terms) shows a good agreement between modelling and data [44]. A more recent study using the GS2 code confirms that TEM is the dominant instability in hot electron plasmas [64]. The quasi-linear electron heat flux is then close to a critical gradient model formulation, provided collisions and density gradient effects are accounted for (Fig.9a). Modelling of heat modulation experiments has been undertaken at JET using Weiland and GLF23 transport models [45]. The collisional Weiland model is able to reproduce experimental data. In particular electron stiffness is found to increase with the ratio of ion to electron power [45] (Fig.9b). On the other hand, the GLF23 model is generally found to reproduce transient experiments less well[45,49].

In summary, although Fig.8 exhibits a strong variability of the stiffness factor, it appears that theory can be reconciled with experiments when using first principle modelling. Still several pending issues remain to be solved. In particular, the question of turbulent transport when several branches coexist remains unclear. This issue will be addressed using turbulence simulations in the future.

## 5. FORMATION OF INTERNAL TRANSPORT BARRIERS

The physics of Internal Transport Barriers (ITB's) is a broad subject that is already covered by several overview papers [65,66,67]. The present section is dedicated to the very specific question of ITB formation. This is a crucial question in terms of power threshold, which is the amount of power that is necessary to produce a barrier. Two key ingredients are known to play a central role in the physics of ITBs: shear flow and magnetic topology. The velocity shear rate will be small in a reactor at the onset of an ITB, so that magnetic shear and Shafranov shift will have to be optimised to trigger the ITB. Attention is focussed here on electron transport barriers, which are well suited to study this physics since the velocity shear rate is naturally small in these plasmas. On the other hand, the physics of barriers in reactor plasmas may be different because the ratio of electron to ion temperature is closer to one.

### 5.1 SHEAR FLOW STABILISATION.

The physics of turbulent transport reduction due to  $E \times B$  shear flow is well documented [68,69,70,71,72,73,74,75]. The interested reader may consult overviews on theory [76] and experiments related to shear flow stabilisation [77]. Stabilisation results essentially from the shearing of turbulent convective cells. An approximate criterion for stabilisation is  $\gamma_E > \gamma_{lin}$  [73], where  $\gamma_E$  is the shear flow rate defined as [74]

$$\gamma_E = \frac{RB_\theta}{B} \frac{d}{dr} \left[ \frac{E_r}{RB_\theta} \right] \quad (9)$$

and  $\gamma_{lin}$  is the maximum linear growth rate. Here  $B_\theta$  is the poloidal magnetic field and  $E_r$  is the

radial electric field. The radial electric field is constrained by the ion force balance equation

$$\frac{e_i E_r}{T_i} = \frac{dn_i}{n_i dr} + (1 - k_{neo}) \frac{dT_i}{T_i dr} + \frac{V_\phi}{n_i dr}, \quad (10)$$

where the number  $k_{neo}$  depends on the collisionality regime and  $V_\phi$  is the ion toroidal velocity. Once a barrier is formed, a positive loop takes place where density and ion temperature gradients increase, thus boosting the velocity shear rate. The situation is different at the onset of the barrier. The torque will be small in a reactor, so that  $V_\phi \approx 0$ . Since typical growth rates are of the order of  $c_s/\alpha$ , it is found that the ratio  $\gamma_E/\gamma_{lin}$  scales as the normalised gyroradius  $\rho^*$ . This ratio is small in present tokamaks and will be even smaller in next step devices. Hence shear flow alone cannot usually trigger an internal transport barrier in absence of torque. A reduction of the linear growth rate is necessary. In that respect, electron transport barriers are interesting since the shear flow rate is small in these plasmas (cold ions, no fuelling and no torque). This property has been verified at JET where a blip of NBI was used in the preheat phase (dominant electron heating) to measure the velocity profile [78,79].

## 5.2. A ROBUST MECHANISM: NEGATIVE MAGNETIC SHEAR AND A STABILISATION.

Negative magnetic shear is known to decrease the interchange drive [80]. This effect is enhanced by the Shafranov shift of magnetic surfaces (also called  $\alpha$  effect,  $\alpha = -q^2 R d\beta/dr$  is a measure of the Shafranov shift) [81,82]. In fact this physics is related to the stability of MHD ballooning modes [83] and the ‘‘access to second stability’’ (see for instance [84]). For electron modes (TEM), it takes a subtle form as it corresponds to a reversal of curvature drift when  $s < -3/8$ . This leads to a fully stable situation in terms of interchange stability [85]. This value also corresponds to a reversal of the curvature pinch velocity (see section 3). Since stabilisation and pinch reversal occur for the same value of the magnetic shear, a reversal of curvature pinch is not observable (in other words, particle pinch should be neoclassical for  $s < -3/8$ ). This stabilisation scheme has been tested with the help of kinetic [86] and fluid simulations. An electron transport barrier appears when magnetic shear is negative, as shown on Fig.10 [87]. This effect is amplified for values of  $\alpha$  of the order of unity. For electron modes, theory predicts stability when  $s < 3 a/5 - 3/8$  [88]. The  $\alpha$  effect was found to be important for barrier triggering in DIII-D, but not in JT-60U or JET [89]. It was shown in the same work that Weiland model does not always predict ITB formation because the effect of magnetic shear is not strong enough. GLF23 model does predict ITB formation. However, the ITB is usually not located at the right minor radius.

Stabilisation at negative magnetic shear is consistent with the onset of an electron barrier at JET during the preheat phase with LHCD [78]. The mechanism is found to work as far as heating power is localised in the core [90]. It is also consistent with the early observation of electron barriers (LHEP mode) on TORE SUPRA [91], FTU [92], TCV [93] and more recently on ASDEX-Upgrade

[94]. Although not the focus of this section, it is worth noting that a similar effect exists for ions, which comes from the shear dependence of the ion curvature averaged over the mode structure  $\lambda_i = \langle \cos(\theta) + (s\theta - \alpha \sin(\theta)) \sin(\theta) \rangle$ . This physics has been studied in detail and will not be addressed further here [see for instance 95].

### 5.3. WHY NEGATIVE MAGNETIC SHEAR CANNOT BE THE ONLY MECHANISM.

An explanation based on negative magnetic shear only cannot explain all type of barriers at JET. There are two reasons at least for that; the role of rational  $q_{min}$  and the coexistence of several barriers. The favourable role of a low order rational value of the minimum safety factor has recently been confirmed in reversed shear plasmas thanks to the observation of Alfvén wave cascades [96,97]. Coexistence of barriers has been observed both in electron and ion channels at JET. A transition is often observed between a single barrier localised at negative shear and a double barrier, when  $q_{min}$  crosses a low order rational number (see Fig. 11). Three explanations have been proposed to explain this behaviour:

- i) the onset of MHD modes located at rational values of  $q$  that generate a localised velocity shear [98]. An alternative is based on a loss of fast ions due to MHD that leads to a shear flow [99].
- ii) turbulent flow generation enhanced close to rational  $q$  values. This explanation does receive some support from electromagnetic turbulence simulations with the CUTIE code [100]. These simulations also show that low wave number modes modify the  $q$  profile near rational values, thus further lowering the magnetic shear locally.
- iii) the existence of gaps in the density of magnetic surfaces where the safety factor is rational (these are places where modes tend to be localised because of resonances). This gap is wider when  $q_{min}$  is close to a low order rational number. Also several gaps may appear simultaneously [101].

The third explanation has been questioned by recent turbulence simulations with the gyrokinetic code GYRO, which do not find any sign of gaps, nor a special role of zero magnetic shear  $s=0$  [102]. The explanation based on MHD does find some support from the correlation observed in JET between ITB formation and MHD activity in positive (optimised) shear plasmas [98]. MHD activity is not always observed in reversed shear plasmas apart from the Alfvén cascade itself. However tearing modes located at  $q=2$  surfaces may be difficult to detect. An explanation based on turbulent dynamo and localised velocity shear is still in discussion and is difficult to verify experimentally, although large transients in the  $E \times B$  flow were observed in TFTR [103].

## CONCLUSION

Progress has been made in understanding particle transport in tokamaks. Theory predicts that both thermo-diffusion and magnetic field curvature contribute to turbulent pinch. Also curvature pinch depends on magnetic shear and the peaking factor decreases with collisionality. These predictions have been tested against experimental results in several devices. Plasmas with peaked density profiles and no Ware pinch were produced in TORE SUPRA and TCV, thus pointing towards the existence

of a turbulent pinch in L-mode. It has been verified also that pinch velocity increases with magnetic shear in JET, TORE SUPRA and TCV L-mode plasmas. In H-mode, density peaking is sensitive to collisionality as found in ASDEX-Upgrade, and JET. At high collisionality, the pinch velocity is close to Ware value, whereas it is larger at low collisionality. This suggests that density profiles in ITER may be more peaked than expected. RF heating is found to flatten density profiles. When collisionality is large, this is interpreted as an increase of the turbulent diffusion coefficient while the pinch velocity stays close to the neoclassical value. For low density plasmas, the interpretation rather relies on the weakening (and may be reversal) of pinch velocity predicted by theory when turbulence move from ion to electron dominant micro-instabilities.

Progress has been made in the development of dimensionless scaling laws and assessment of transport models using heat modulation experiments. Recent experiments on DIII-D and JET show that the dimensionless scaling law of energy confinement is consistent with electrostatic turbulent transport. Low collisionality is found to improve the confinement. This behaviour remains unexplained. These results lead to a prediction of confinement that will be better than expected in ITER in the domain of high beta plasmas. Heat modulation experiments have been undertaken at JET, ASDEX-Upgrade, TORE SUPRA, FTU and TCV. These experiments have been analysed using a critical gradient transport model, stability analysis and predictive modelling. Instability thresholds are found to be in the expected range for micro-instabilities in tokamaks. Electron stiffness is found to cover a wide range of variation. Still the Weiland transport model is able to reproduce experimental data both in ASDEX-Upgrade and JET. Also kinetic stability analysis is consistent with transport modelling and critical gradient model for hot electron plasmas in ASDEX-Upgrade. At JET a correlation was found between electron stiffness and the ion temperature gradient length. This observation suggests that some interplay exists between electron and ion heat channels. The applicability of a critical gradient model in the case where ion and electron modes are linearly unstable will thus have to be further investigated. No firm conclusion can yet be drawn regarding profile stiffness in ITER.

Finally the question of triggering Internal Transport Barriers has been addressed by analysing electron transport barriers, which are characterised by low mean shear flow. It is confirmed that negative magnetic shear, combined with the Shafranov shift, is a robust stabilising mechanism. However, some well established features of internal barriers are not explained by theory, in particular the role of rational values of the minimum safety factor and the existence of multiple barriers observed at JET. Tailoring the current profile will likely provide the most efficient way to produce internal transport barriers in ITER, since the mean velocity shear rate will be moderate in these plasmas. This will require efficient tools to modify the shape of plasma current density.

## REFERENCES

- [1]. W. Horton, Rev. Mod. Physics **71**, 735 (1999).
- [2]. J. Weiland, “*Collective Modes in Inhomogeneous Plasmas*”, IOP, 2000.
- [3]. H. Nordman, J. Weiland, A. Jarmen, Nucl. Fusion **30**, 983 (1990)

- [4]. R.E. Waltz, G.M. Staebler, W. Dorland, et al., *Phys. Plasmas* **4**, 2482 (1997).
- [5]. B.B. Kadomtsev, *Sov. J. Plasma Phys.* **n1**, 295 (1975).
- [6]. J.W. Connor, and J.B. Taylor, *Nucl. Fusion* **n17**, 1047 (1977).
- [7]. P.H. Diamond et al., in *Proceedings of the 17th IAEA Fusion Energy Conference, IAEACN-69/TH3/1* 1998.
- [8]. G. Falchetto and M. Ottaviani, *Physical Review Letters* **92** 25002 (2004).
- [9]. A.A. Ware *Phys. Rev. Lett.* **25**, 916 (1970).
- [10]. B. Coppi and C. Spight, *Phys. Rev. Lett.* **41**, 551 (1978).
- [11]. W.Tang et al., *Phys. Fluids* **29**, 3715 (1986) 22
- [12]. V.V. Yankov, *JETP Lett.* **60**, 171 (1994).
- [13]. M.B. Isichenko, A.V. Gruzinov, P.H. Diamond, *Phys. Rev. Lett.* **74**, 4436 (1996).
- [14]. D.R. Baker and M.N. Rosenbluth, *Phys. Plasmas* **5**, 2936 (1998).
- [15]. V. Naulin, J. Nycander, and J. Juul Rasmussen, *Phys. Rev. Lett.* **81**, 4148 (1998).
- [16]. H. Nordman, J. Weiland, A. Jarmen, *Nucl. Fusion* **30**, 983 (1990)
- [17]. C. Angioni, A.G. Peeters, G.V. Pereverzev et al., *Phys. Plasmas* **10**, 3225 (2003). C. Angioni, A.G. Peeters, G.V. Pereverzev et al., *Phys Rev Lett.* **90**, 205003-1 (2003).
- [18]. X. Garbet, L. Garzotti, P. Mantica, et al., *Phys. Rev. Lett.* **91**, 035001 (2003) .
- [19]. J. Stober, C. Fuchs, O. Gruber, et al., *Nuclear Fusion* **41**, 1535 (2001).
- [20]. M.Valovic, J. Rapp, J.G. Cordey, et al., *Plasma Physics and Controlled Fusion* **44**, 1911 (2000).
- [21]. H. Weisen et al, *Nuclear Fusion* **42**, 136 (2002).
- [22]. M. Z. Tokar, J. Ongena, B. Unterberg, and R. R. Weynants , *Phys. Rev. Lett.* **84**, 895 (2000).
- [23]. G.T. Hoang, C. Bourdelle, B. Pegourie, et al., *Phys. Rev. Lett.* **90**, 155002 (2003)
- [24]. A. Zabolotsky, H. Weisen , and TCV Team, *Plasma Phys. Control. Fusion* **45**, 735 (2003).
- [25]. L Garzotti, X Garbet, P Mantica, et al., *Nucl. Fusion* **43**, 1829 (2003).
- [26]. H. Weisen et al., in *Proceedings of the 31st EPS Conference on Plasma Physics, London, 2004*.
- [27]. M. Valovic, R. Budny, L. Garzotti, et al., submitted to *Plasma Phys. Control. Fusion*.
- [28]. K-D Zastrow et al., in *Proceedings of the 31st EPS Conference on Plasma Physics, London, 2004*, to be submitted to *Plasma Phys. Control. Fusion*.
- [29]. I. Voitsekhovitch et al., in *Proceedings of the 31st EPS Conference on Plasma Physics, London, 2004*.
- [30]. H. Weisen, A. Zabolotsky, X. Garbet, et al., *Plasma Phys. Control. Fusion* **46**, 751 (2004)
- [31]. T. Hoang et al., submitted to *Phys. Rev. Lett.*
- [32]. J. Stober, R. Dux, O. Gruber, et al., *Nucl. Fusion* **43**, 1265 (2003).
- [33]. C. Angioni et al., *Nucl. Fusion* **44**, 827 (2004).
- [34]. M. E. Puaitti, M. Valisa, M. Mattioli, et al., *Plasma Phys. Control. Fusion* **44**, 2135 (2002).
- [35]. D.C. McDonald, et al. *Plasma Phys. Cont. Fusion* **n46** A215 (2004).
- [36]. C.C. Petty et al. *Phys. Plasmas* **11**, 2514 (2004). 23
- [37]. G. Cordey et al., *Nucl. Fusion* **43**, 670 (2003).
- [38]. P.H. Rebut, P.P. Lallia, M.L. Watkins, in *Plasma Physics and Controlled Nuclear Fusion*

- Research 1988 (Proc. 12th Int. Conf. Nice, 1988), Vol.II, IAEA, Vienna (1989), 191.
- [39]. M. Kotschenreuther, W. Dorland, M.A. Beer, and G.W. Hammett, *Phys. Plasmas* **2**, 2381 (1995).
  - [40]. M. Erba et al., *Plasma Phys. Contr. Fusion* **39**, 261 (1997).
  - [41]. P. Zhu, G. Bateman, A.H. Kritz, W. Horton, *Phys. Plasmas* **7**, 2898 (2000).
  - [42]. M. Ottaviani, W. Horton, M. Erba, *Plasma Phys. Cont. Fus.* **39**, 1461 (1997).
  - [43]. V. Parail et al., *Nucl. Fusion* **37**, 481 (1997).
  - [44]. G. Tardini et al, *Nucl. Fusion* **42**, L11 (2002).
  - [45]. P. Mantica et al., in Proceedings of the 31st EPS Conference on Plasma Physics, London, 2004. P. Mantica et al., in Proceedings of the 30rd EPS Conference on Plasma Physics, St-Petersburg, 2003.
  - [46]. B. Coppi and N. Sharky, *Nucl. Fusion* **21**, 1363 (1981).
  - [47]. F. Ryter, F. Leuterer, G. Pereverzev, et al., *Phys. Rev. Lett.* **86**, 2325 (2001).
  - [48]. G.T. Hoang, C. Bourdelle, X. Garbet, et al., *Phys. Rev. Lett.* **87**, 125001 (2001).
  - [49]. P. Mantica, et al., *Plasma Physics and Controlled Fusion* **44**, 2185 (2002).
  - [50]. D.R. Baker, et al., *Phys. Plasmas* **8**, 4128 (2001).
  - [51]. A.G. Peeters, *Nucl. Fusion* **42**, 1376 (2002).
  - [52]. D.R. Mikkelsen, et al., *Nucl. Fusion* **43**, 30 (2003).
  - [53]. M. Kotschenreuther, W. Dorland, M.A. Beer, et al., *Phys. Plasmas* **2**, 2381 (1995).
  - [54]. C. Bourdelle et al., *Nucl. Fusion* **42**, 892 (2002).
  - [55]. F. Imbeaux, F. Ryter and X. Garbet, *Plasma Physics and Controlled Fusion* **43**, 1503 (2001).
  - [56]. F. Ryter et al., *Nucl. Fusion* **43**, 1396 (2003).
  - [57]. P. Mantica, in proceedings of the 19th IAEA Fusion Energy Conference, Lyon 2002.
  - [58]. Y. Camenen, A. Pochelon, F. Ryter, S. Coda “Electron heat transport studies under intense EC heating in TCV”, IAEA Technical Meeting on ECRH Physics and Technology for ITER (F1-TM-26015), Kloster Seeon, Germany, July 2003. CRPP Lausanne Report LRP 768/03 (2003).
  - [59]. X. Garbet, P. Mantica, F. Ryter, et al., to appear in *Plasma Physics and Control. Fusion*.
  - [60]. J. DeBoo et al., *Nucl. Fusion* **39**, 1935 (1999). 24
  - [61]. O.J.W.F. Kardaun et al, 2001 Fusion Energy 2000 (Proc. 18th Int. conf. Sorrento, 2002) (Vienna: IAEA)
  - [62]. G. Cordey, et al., in Proceedings of the 31st EPS Conference on Plasma Physics, London, 2004.
  - [63]. C.C. Petty, J.E. Kinsey, T.C. Luce, *Phys. Plasmas* **11**, 1011 (2004)
  - [64]. M. Apostoliceanu, C. Angioni, A.G. Peeters et al., to be submitted.
  - [65]. R C Wolf, *Plasma Phys. Control. Fusion* **45**, R1 (2003).
  - [66]. J.W. Connor, T. Fukuda, X. Garbet, et al., *Nucl. Fusion* **44**, R1 (2004).
  - [67]. C. Challis, submitted to *Plasma Physics and Control. Fusion*.
  - [68]. S-I Itoh, K. Itoh *Phys. Rev. Lett.* **60**, 2276 (1988).
  - [69]. K.C. Shaing, E.C. Crume, *Phys. Rev. Letters* **63**, 2369 (1989).
  - [70]. H. Biglari, P.H. Diamond, and P.W. Terry *Phys. Fluids B* **2**, 1 (1990).

- [71]. S. Hamaguchi and W. Horton, *Phys. Fluids B* **4**, 319 (1992).
- [72]. G.M. Staebler, F.L. Hinton, J.C. Wiley, R.R. Dominguez, C.M. Greenfield, P. Gohil, T.K. Kurki-Suonio, T.H. Osborne, *Phys. Plasmas* **1**, 909 (1994).
- [73]. R.E. Waltz, G.D. Kerbel, J. Milovitch, *Phys. Plasmas* **1**, 2229 (1994).
- [74]. T.S. Hahm and K.H. Burrell, *Phys. Plasmas* **2**, 1648 (1995).
- [75]. C. Figarella et al., *Phys. Rev. Lett.* **90**, 015002 (2003).
- [76]. P.W. Terry, *Rev. Mod. Phys.* **72**, 109 (2000).
- [77]. K.H. Burrell, *Phys. Plasmas* **6**, 4418 (1999).
- [78]. G M D Hogeweyj et al., *Plasma Phys. Control. Fusion* **44**, 1155 (2002).
- [79]. G D Conway et al., *Plasma Phys. Control. Fusion* **44**, 1167(2002).
- [80]. J.F. Drake, Y.T. Lau, P.N. Guzdar, et al., *Phys. Rev. Lett.* **77**, 494 (1996).
- [81]. M. Beer, G.W. Hammett, G. Rewoldt, et al., *Phys. Plasmas* **4**, 1792 (1997).
- [82]. C. Bourdelle, W. Dorland, X. Garbet, et al., *Phys. Plasmas* **10**, 2881 (2003).
- [83]. J. W. Connor, R.J. Hastie, and J.B. Taylor, *Phys. Rev. Lett.* **40**, 396 (1978).
- [84]. B. Coppi, A. Ferreira, J-W-K Mark, J.J. Ramos, *Nucl. Fusion* **19**, 715 (1979)
- [85]. B.B. Kadomtsev, O.P. Pogutse, *Reviews of Plasma Physics*, edited by M.A. Leontovitch (Consultant Bureau, New York, 1970) Vol. 5, p. 249.
- [86]. A. Bottino, PHD thesis, Lausanne 2004.
- [87]. Y. Baranov et al., *Plasma Physics and Control. Fusion* **46**, 1181 (2004).
- [88]. P. Maget, X. Garbet, A. Géraud, E Joffrin *Nucl. Fusion* **39**, 949 (1999).
- [89]. T. Tala, et al., submitted to *Plasma Physics and Control. Fusion*. **25**
- [90]. N. Kirneva et al., in *Proceedings of 31st EPS Conference on Plasma Physics*, London, 2004.
- [91]. D. Moreau and the TORE SUPRA Team., in *proceedings of the 14th International Conference on Plasma Physics and Controlled Nuclear Fusion Research*, Würzburg, 1992, (IAEA,Vienna, 1994), vol.I, p.649. X Litaudon, T Aniel, Y Baranov, et al., *Plasma Physics and Cont. Fusion* **38**, 1603 (1996).
- [92]. P. Buratti, et al., *Phys. Rev. Lett.* **82**, 560 (1999).
- [93]. T.P. Goodman et al., et al. *Nucl. Fusion* **43**, 1619 (2003).
- [94]. F. Leuterer et al., *Nuclear Fusion* **43**, 1329 (2003).
- [95]. R. Budny et al., in *Proceedings of 30th EPS Conference on Plasma. Physics and Controlled Fusion*, St Petersburg, 2003.
- [96]. S. Sharapov, B. Alper, H.L. Berk, et al., *Phys. Plasmas* **9**, 2027 (2002).
- [97]. E. Joffrin C.D. Challis, G.D. Conway, et al., *Nucl. Fusion* **43**, 1167 (2003).
- [98]. E. Joffrin et al., *Plasma Physics and Control. Fusion* **44**, 1739 (2002).
- [99]. S. Guenter et al., in *Proceedings of 28th EPS Conference on Plasma. Physics and Controlled Fusion* **25A**, 1006 (2000).
- [100]. A Thyagaraja, P.J. Knight and N. Loureiro in *European Journal of Mechanics B/Fluids* **23**,475 (2004)
- [101]. X. Garbet, Y. Baranov, G. Bateman, et al., *Nuclear Fusion* **43**, 975 (2003).
- [102]. J. Candy, R. Waltz, M.N. Rosenbluth, *Phys. Plasmas* **9**, 1938 (2004).
- [103]. R.E. Bell et al., *Phys. Rev. Lett.* **81**, 1429 (1998).

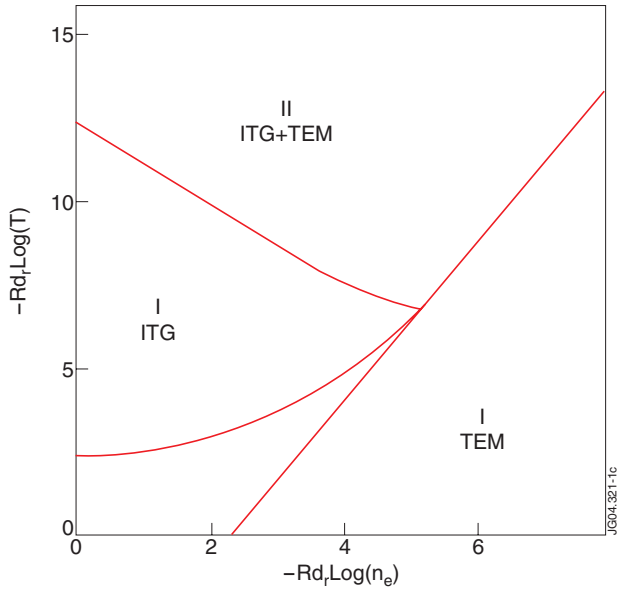


Figure 1: Stability diagram of ITG/TEM modes. Roman numbers indicate the number of unstable modes. Electron and ion temperatures are equal.

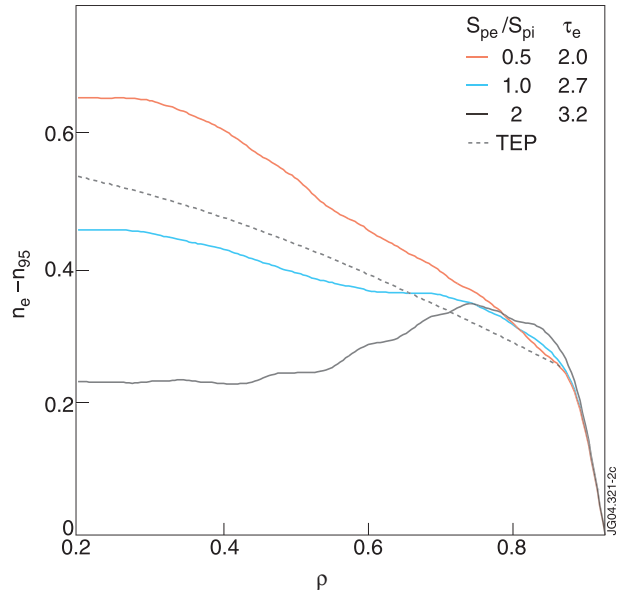


Figure 2: Density profiles calculated with TRB turbulence simulations when varying the ratio of electron to ion heating  $S_{pe}/S_{pi}=0.5, 1$  and  $2$ . The corresponding values of  $te = \sqrt{T_e}/\sqrt{T_i}$  at  $r/a=0.5$  are indicated [18].

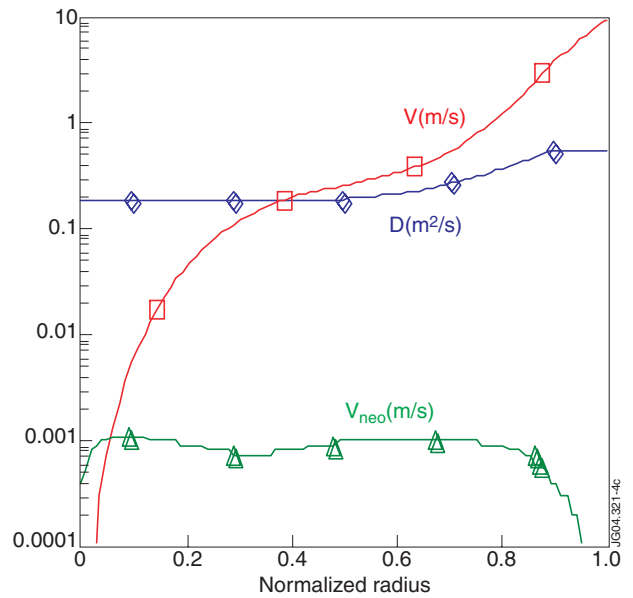
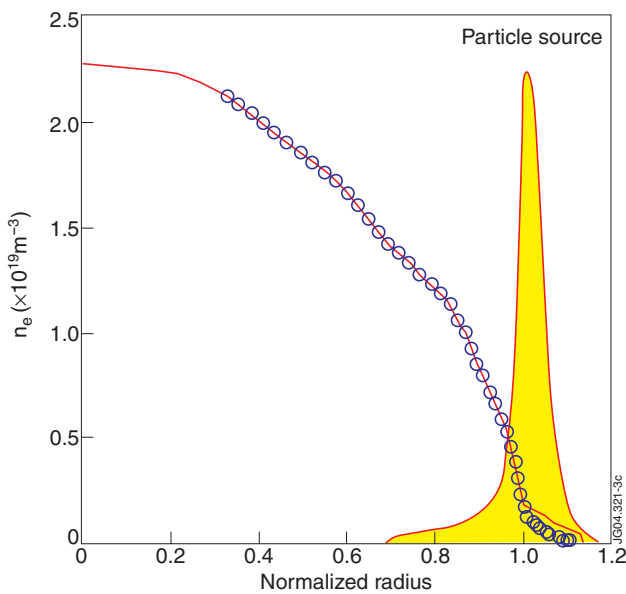


Figure 3: 1D simulation of discharge #30428 in TORE SUPRA, at  $t=30s$ . a) Density profile (full line: simulation; circles: reflectometry measurements). b) Particle pinch velocity (full line/squares, in unit  $m.s^{-1}$ ) and diffusion coefficient (full line/diamonds, in unit  $m^2.s^{-1}$ ) used to reproduce measured density profile. Triangles show the profile of neoclassical pinch velocity ([23]).

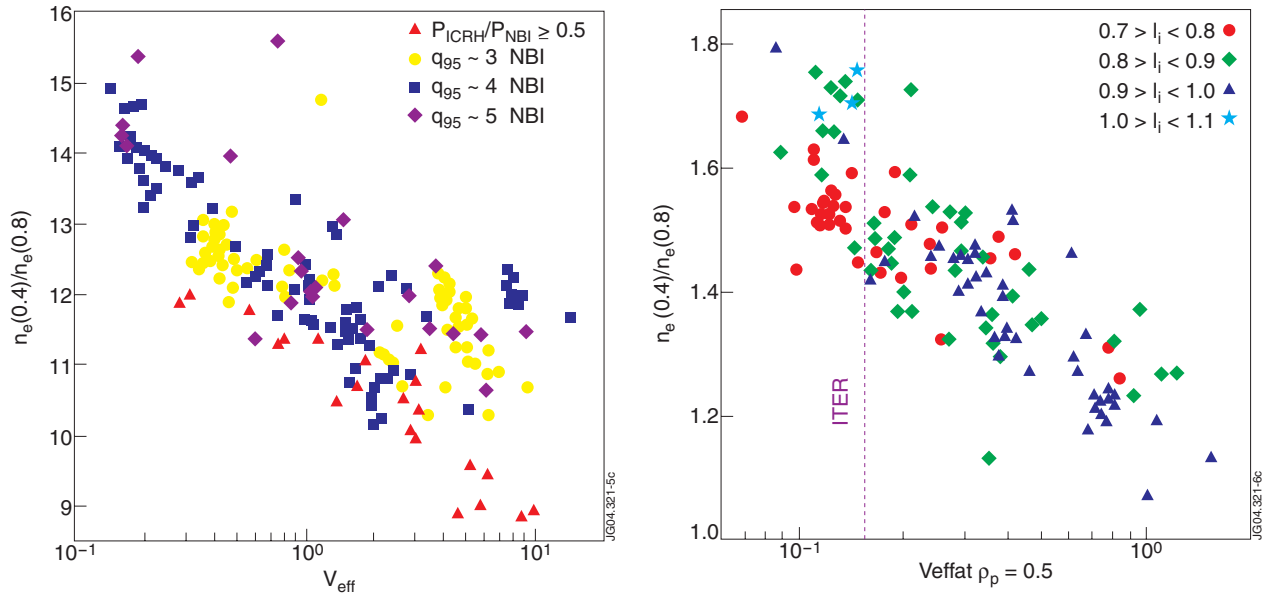


Figure 4: Density peaking versus  $v_{eff}=(5/2)^{1/2} v_{ei}R/c_s$  in ASDEX-Upgrade [17] and JET [26]. Plasmas are in H-mode.

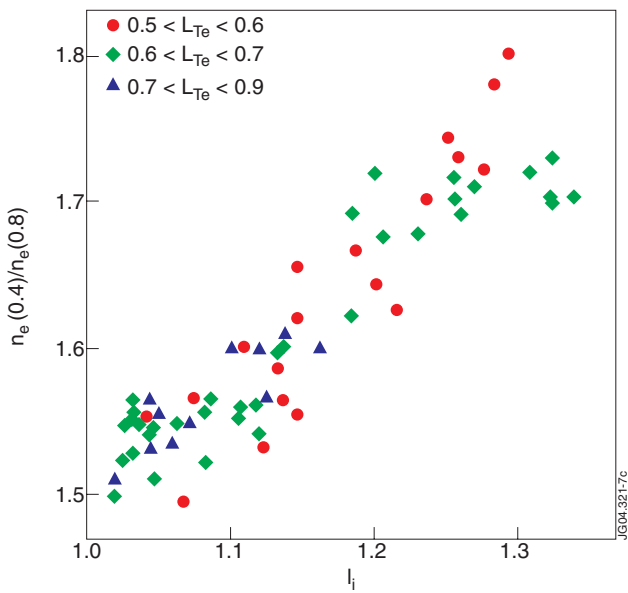


Figure 5: Peakedness of density profiles in JET versus internal inductance for different

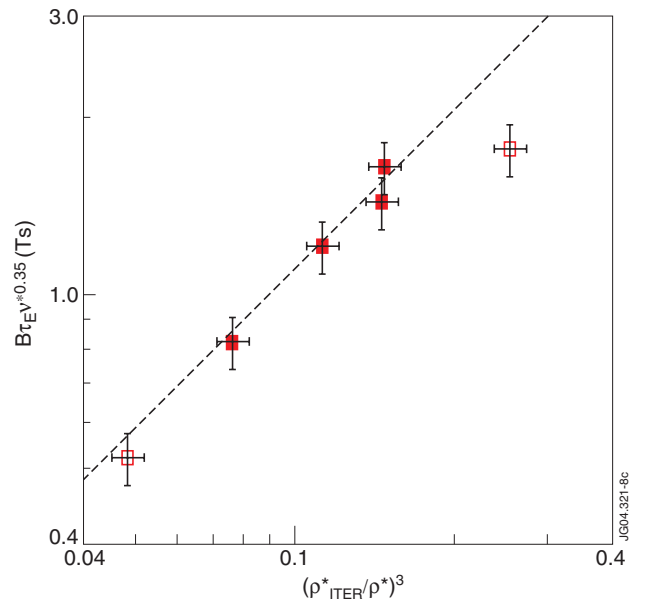


Figure 6: Normalised confinement time  $v^{*0.35} B \tau_E$  versus  $[\rho^*/\rho^*_{ITER}]^3$  in JET plasmas [62].

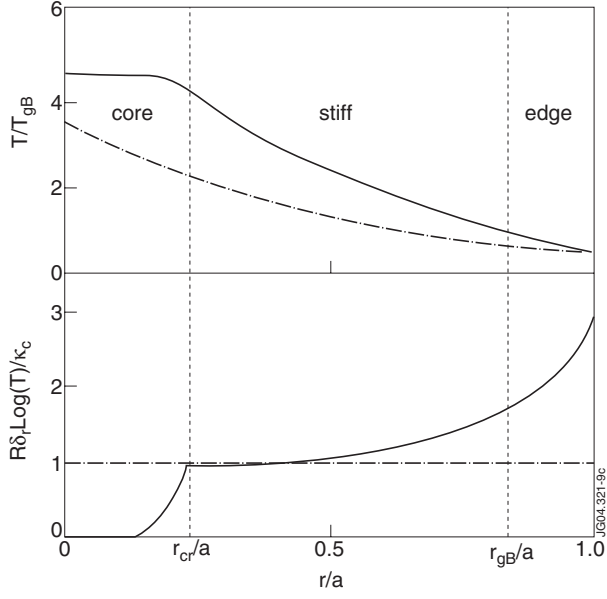


Figure 7: Calculated normalised temperature and its logarithmic derivative. Dashed line corresponds to a Profile that is marginally stable everywhere

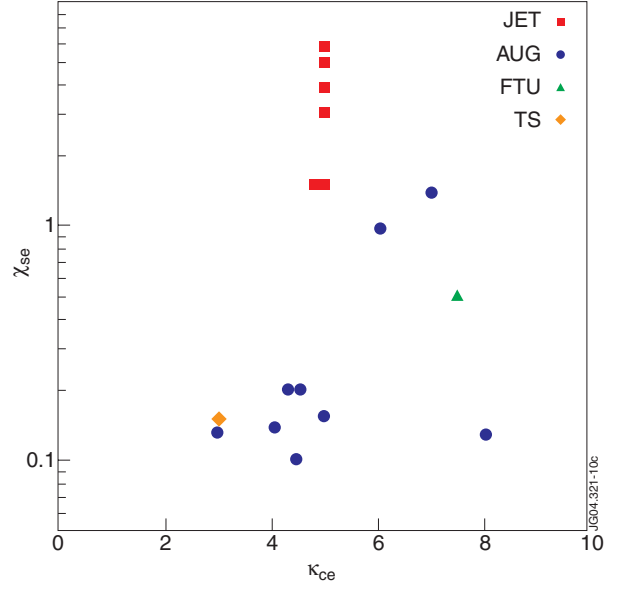


Figure 8: Electron stiffness  $\chi_{s,e}$  vs threshold  $\kappa_{c,e}$  deduced from modulation experiments in ASDEX-Upgrade, JET,

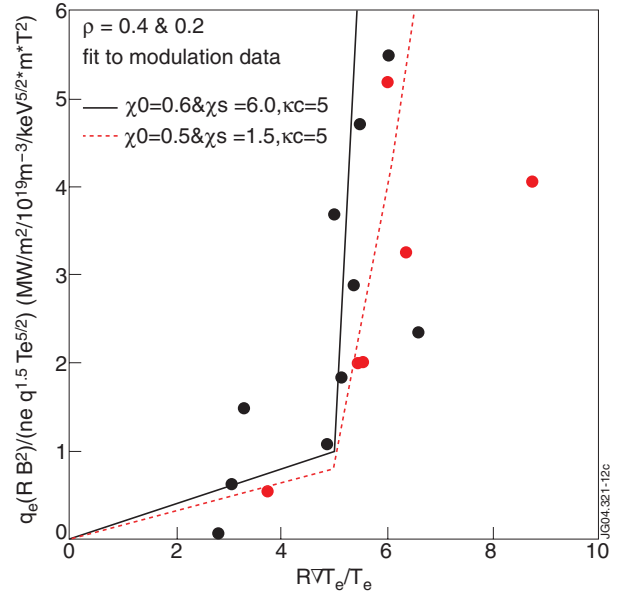
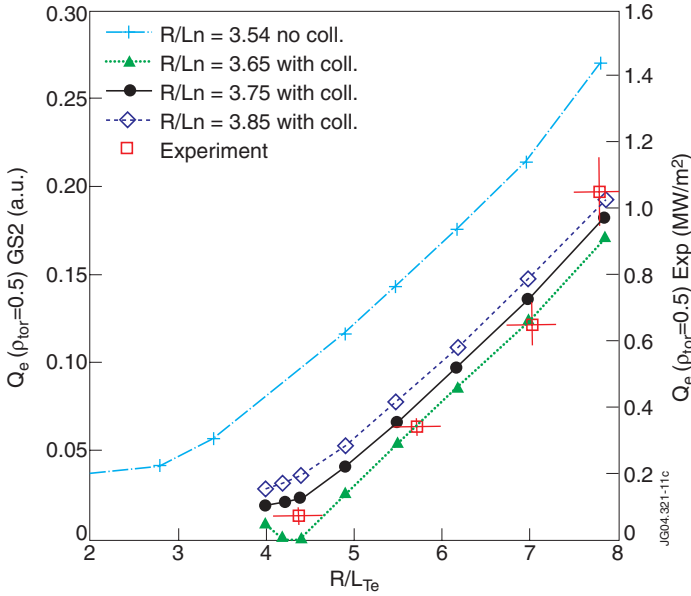


Figure 9: Left panel: electron heat flux versus logarithmic gradient of electron temperature. Comparison between a quasi-linear estimate calculated with the GS2 stability code and experimental value in ASDEX-Upgrade (from [64]). Right panel: electron heat vs logarithmic gradient of electron temperature in heat modulation experiments at JET with dominant electron heating (red) and significant ion heating (black) (from [45])

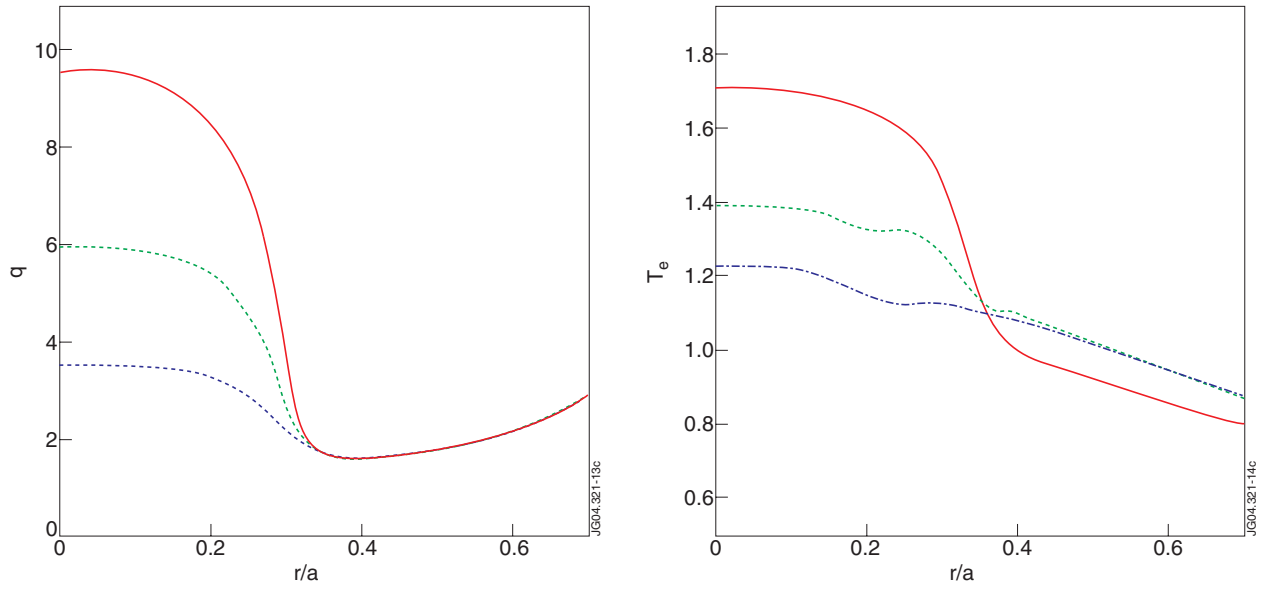


Figure 10: Profiles of safety factor, and electron temperature calculated with the TRB Turbulence code [87].

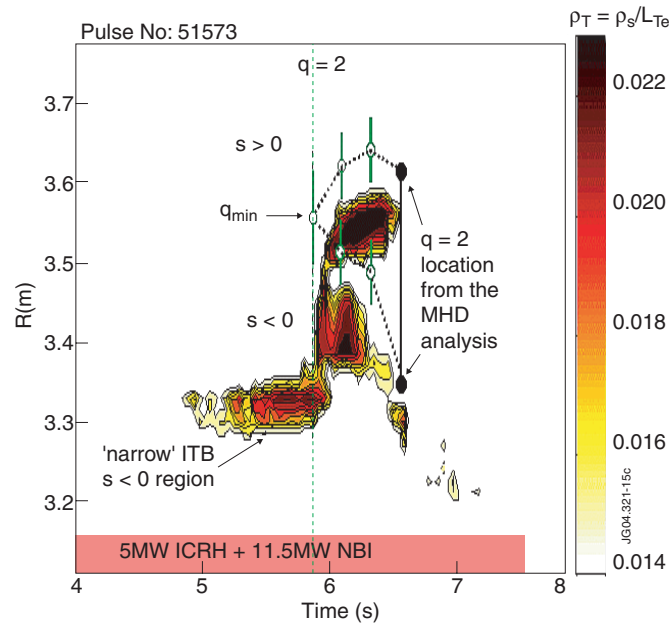


Figure 11: Contours of  $\rho_T^* = \rho_s / L_{Te}$  of the JET pulse No.51573 (from [98]).